Celal Bayar University Journal of Science

Numerical Simulation on Balistic Performance of SiC/Light Metal Laminated Composite Armor against .30 APM2

Saim Kural[1*], Mehmet Ayvaz[2]

[1*] Department of Mechanical Engineering, Manisa Celal Bayar University, Manisa 45140, Turkey
[2] Vocational School Of Manisa Technical Sciences, Manisa Celal Bayar University, Manisa 45140, Turkey
*saim.kural@cbu.edu.tr
*Orcid: 0000-0003-1722-6252

Received: 20 July 2020
Accepted: 5 December 2020
DOI: 10.18466/cbayarfbe.771866

Abstract

Ceramic/metal laminated composite armor systems have great importance and potential in defence technology due to their high ballistic performance and lightweight. In this study, it was aimed to determine the ballistic performances, limits, and perforation types of light metals (with densities below 5.0 g/cm^3) used as ductile backing plates in laminated composite armor systems. In the numerical analysis, SiC tiles of 5 and 10 mm thickness were used as the front layer. Al5083-H116, Mg AZ31B, and Ti6Al4V light metal alloys in different thicknesses were used as the backing layer. While using the Johnson and Holmquist (JH-1) material model in SiC ceramic tiles, the Johnson-Cook (JC) material model was applied for ".30 APM2" bullet components and metal layers. The analyzes were performed with Ansys/Autodyn software. As a result of the simulations, among all the laminated armor systems providing full protection against ".30 APM2" ballistic threats with a collision speed of 878 m/s, the lowest areal density was determined as 54.245 kg/m^2 in 10 mm SiC/5 mm Ti6Al4V laminated composite armor.

Keywords: Ballistic Performance; Laminated Composite; Finite Element Analysis; Ti6Al4V; Mg AZ31B.

1. Introduction

Steel and its alloys are widely used as armor material due to their low cost, strength, and hardness that can be improved by heat treatments. However, in addition to performing ballistic protection, armor material should not restrict the mobility of target to move away from repeated ballistic threats. Also, reducing the weight of the armor can help decrease energy.[1]. For the use of low weight materials as armor, ballistic performances of light metals are examined and tried to be developed. For this purpose, the most frequently studied alloys are age-hardenable aluminum alloys.

Another aluminum alloy known to be widely used in armored vehicles is AA5083, whose strength can be increased by deformation hardening [2]. Borvik et al. investigated the ballistic behavior of 15-30 mm thick AA5083 armors with a diameter of 20 mm and a length of 98 mm with a conical tip steel projectile by experimental studies [3]. Ballistic limit speeds of AA5083 armors of 15, 20, 25, and 30 mm thickness were 216.8, 249.0, 256.6, and 309.7 respectively. In the study carried out with the finite element method using the same parameters in the empirical study of Borvik et al. [3], ballistic limit velocities were calculated by showing a maximum ~5 % deviation to experimental results [4]. In the tests, ballistic limit speeds of AA5083 plates with 20, 2x20, and 3x20 mm layer numbers and thicknesses were obtained as 492, 722, and 912 m/s, respectively, against 7.62 mm APM2 bullets [5]. Magnesium alloys, especially Mg AZ31, whose density is 35 % lower than aluminum, have a high potential for light armor systems [6]. Moreover, in experimental studies, the ballistic limit velocities of Mg AZ31 and AA5083 armor plates with the same field density (~ 135.2 kg/m^2) were determined as 863 and 853 m/s, respectively [7]. Another light metal used as armor material is titanium alloys [8]. By using Ti6Al4V alloy armor, ~30-40% weight reduction is achieved compared to Rolled Homogeneous Armor (RHA) usage [9]. Also, like steel alloys, it is possible to increase the ballistic performances of titanium alloys [10].

In ballistic protection systems, the desired ballistic protection level cannot be achieved against most ballistic threats by using monolithic metallic armor. For this reason, laminated composite armor plates are used.

Celal Bayar University Journal of Science
Volume 16, Issue 4, 2020, p 409-418
Doi: 10.18466/cbayarfbe.771866

laminated composite armors are obtained by placing ceramic tiles on the impact surface of the deformable and energy absorber armor materials [11]. Determining the penetration and perforation behavior of laminated composite armors with empirical ballistic tests is very costly. For this reason, mathematical models are widely used in the solution of this ballistic physical problem. In ceramic materials, the fracture conoid formed by the impact of the bullet was first modeled by Florence [12]. Alekseevskii [13] and Tate [14] mathematically modeled penetration of the bullet into the armor plate. Analytical models explaining the ballistic behavior of the backing plate and the deformation occurring in this plate were developed by Woodward [15] and Reijer [16]. The penetration stages of the projectile into ceramic-metal laminated composite armors were modeled by Zaera and Sanchez-Galvez [17] based on the models of Alekseevskii [13], Tate [14], Woodward [15] and Reijer [16]. Chocron and Galvez [18] developed models for composite armors with ceramic/polymer composite layers. Feli et al. [19] developed an analytical model to explain the ballistic behavior of ceramic/metal composite armors, considering the deformation and erosion of the projectile tip.

SiC is widely used in ballistic protection systems. However, there are insufficient models in the literature reporting how ballistic performance of SiC/metal laminated composite armor. The ballistic behavior and performance of either monolithic SiC tiles [20] or SiC/metal composite armors against non-standard projectiles were modeled and investigated [21]. Also, to date, the ballistic performance, especially Ti6Al4V and Mg AZ31B light metal alloys, with ceramic layering, has not been reported. In this study, ballistic behavior and performance of SiC/light metal alloy (AA5083, Ti6Al4V, Mg AZ31B) laminated composite armor plates against standard ".30 APM2" were analyzed and optimum thicknesses of the layers were determined.

2. Numerical Methods and Materials Models

Finite element analyzes (FEA) of impact tests were carried out on a 2D axisymmetric model using ANSYS AutoDYN software. The dimensions of our model can be seen in Figure 1. For model, the armor plates were considered fixed from the right-hand side. In addition, for analysis precision, the regions where high collision energy took place were divided into 5 surfaces to create different sized mesh. Mesh element sizes and mesh structures can be seen in Figure 2. This mesh structure and optimizations were determined by obtaining results consistent with experimental results in Borvik at al.[4]. In armors with various thickness, the number of mesh elements and nodes for each thickness was modeled as different. However, since the size of the mesh element was determined for each field with "behavior: hard", the same size element was used for that area.

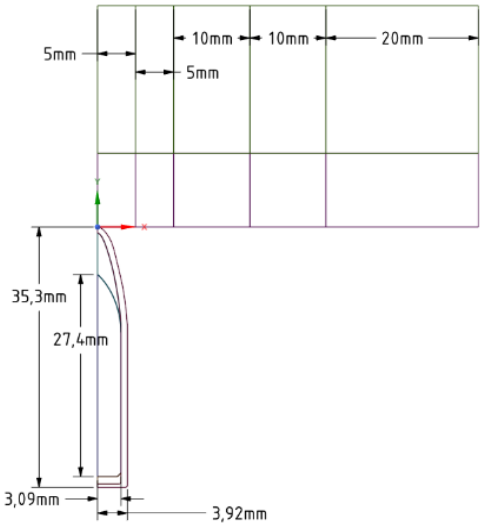

Figure 1. Model dimensions

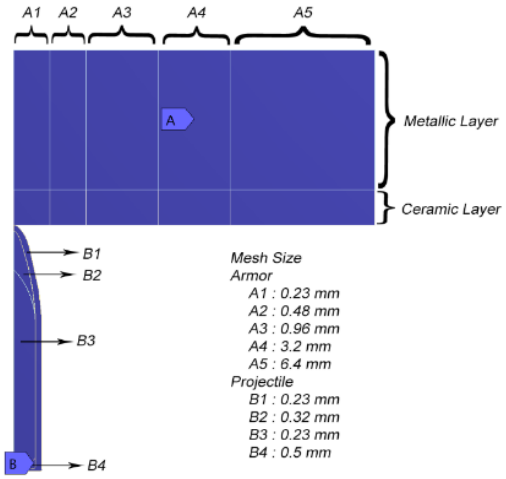

Figure 2. Mesh element sizes and mesh structure

Johnson-Cook strength model was used for Steel 4340 projectile core, and Al 5083-H116 targets in explicit analyses. This model explains the material behavior under penetration conditions, encountered in problems related to high temperature - stress - strain rate and hyper velocity effects [22]. This model is widely used to solve ballistic problems.The Steinberg-Guinan strength model calculates the yield modulus based on effective plastic deformation, pressure, and temperature, which increases with increasing pressure and decreasing with increasing temperature. Table 1 shows the material properties of the projectile and targets for the models used. Material models were used from AutoDYN standard material library. Johnson-Holmquist failure model were used for SiC, Johnson-Cook failure model were used for Steel 4340 and Al5083-H116. For failure models, values in the AutoDYN material library were used.

Table 1. Mechanical properties of comparison model

Material Name	Reference Density (kg/m3)	Equation of State		Strength Model	
Al5053-H116	2700	**Linear**		**Johnson-Cook**	
		Bulk Modulus(MPa)	$5.833x10^4$	Shear Modulus(MPa)	$2.692x10^4$
		Reference Temperature(K	293.00	Yield Stress(MPa)	$1.67x10^2$
		Specific Heat(J/kgK)	910.000122	Hardening Constant(MPa)	$5.96x10^2$
		Thermal Cond. (J/mKs)	117.00	Hardening Exponent.	0.551
				Strain Rate Constant.	0.001
				Thermal Softening Exponent.	0.859
				Melting Temperature(K).	893
				Ref. Strain Rate(/s).	1
				Strain Rate Correction.	1^{st} Order
Steel 4340	7830	**Linear**		**Johnson Cook**	
		Bulk Modulus(MPa)	$1.59x10^5$	Shear Modulus(MPa)	$7.7x10^4$
		Reference Temperature(K	300.00	Yield Stress(MPa)	$7.92x10^2$
		Specific Heat(J/kgK)	477.000092	Hardening Constant(MPa)	$5.1x10^2$
				Hardening Exponent	0.26
				Strain Rate Constant	0.014
				Thermal Softening Exponent	1.03
				Melting Temperature(K)	1793
				Ref. Strain Rate(s^{-1})	1
				Strain Rate Correction	1^{st} Order
Brass	8450	**Shock**		None	
		Gruneisen Coefficient	2.04		
		Parameter C1(m s^{-1})	$3.726x10^3$		
		Parameter S1	1.434		
Lead	11340	**Shock**		**The Steinberg-Guinan**	
		Gruneisen Coefficient	2.74	Shear Modulus(MPa)	$8.6x10^3$
		Parameter C1(m s^{-1})	$2.006x10^3$	Yield Stress(MPa)	$8.0x10^2$
		Parameter S1	1.429	Maximum Yield Stress(MP	$1x10^2$
				Hardening Constant	110
				Hardening Exponent	0.52
				Derivative dG/dP	1
				Deriv. dG/dT (MPa K^{-1})	-9.976
				Deriv. dY/dP	$9.304x10^{-4}$
				Melting Temperature (K)	760
SiC	3215	**Polynomial**		**Johnson-Holmquist**	
		Parameter A1(kPa)	$2.2x10^8$	Shear Modulus(kPa)	$1.935x10^8$
		Parameter A2(kPa)	$3.61x10^8$	Model	JH-1
		Parameter T1(kPa)	$2.2x10^8$	HEL(kPa)	$1.17x10^7$
		Ref. Temp. (K)	293	S1(kPa)	$7.1x10^6$
				P1(kPa)	$2.5x10^6$
				S2(kPa)	$1.22x10^7$
				P2(kPa)	$1x10^7$
				Strain Rate Constant	0.009

Detailed results for comparison, were shown in Table 2. The results in the table clearly show that the FEM analyzes performed is quite compatible with the experimental results. Only one result of FEM analyses (480 m/s striking velocity case), residual velocity was obtained 110.37 m/s, while in the experimental result, the projectile was stopped in response to this speed. This result is expected because the Johnson-Cook strength model is more suitable for high speeds.

Table 2. Comparison of this study with the experimental study of Borvik et al. [5]

Armor			Striking Velocity [m/s]	This Study Residual Velocity [m/s]	Børvik et al.,2010 Residual Velocity [m/s]	% Difference Between Simulation and Experiment
1st Metal Layer Thickness [mm]	2nd Metal Layer Thickness [mm]	3rd Metal Layer Thickness [mm]				
20	0	0	480.0	110.37	0.0000000	N/A
20	0	0	822.4	701.15	694.3000000	0.986605214
20	20	0	669.8	0.00	0.0000000	0
20	20	0	866.3	472.90	486.2000000	-2.735499794
20	20	20	905.6	0.00	0.0000000	0
20	20	20	955.7	254.23	255.4000000	-0.458104933

After correction of model and mesh structure, different armor materials tested against ".30 APM2" ballistic threats with a collision speed of 878 m/s. The ballistic performances, limits, and perforation types of light metals (with densities below 5.0 g/cm3) used as ductile backing plates in laminated composite armor systems. In the numerical analysis, SiC tiles of 5 and 10 mm thickness were used as the front layer. Al5083-H116, Mg AZ31B, and Ti6Al4V light metal alloys in different thicknesses were used as the backing layer. While using the Johnson and Holmquist (JH-1) strength model in SiC ceramic tiles, the Johnson-Cook (JC) strength model was applied for ".30 APM2" bullet core and St 4340, von Mises strength model was applied for Mg AZ31B, and Steinberg Guinan strength model was applied for Ti6Al4V metal layers.

Johnson-Holmquist strength model uses to model brittle materials (glass, ceramics) subjected to large pressures, shear strain, and high strain rates. This model is a combined plasticity and damage model. According to this model, yielding is based on micro-crack growth instead of dislocation movement (metallic plasticity). The von Mises strength model has a fixed value of yield stress just as the original Von-Mises precursors. As a result, the Von-Mises cylinder has a fixed radius. The conditions lying in the cylinder are flexible and the conditions on the surface of the cylinder are plastic.

$$(\sigma_1 - \sigma_2)^2 + (\sigma_2 - \sigma_3)^2 + (\sigma_3 - \sigma_1)^2 = 2Y^2 \quad \textbf{(2.1)}$$

Failure criteria were chosen Hydro (Pmin) for the Mg AZ31 and Ti6AL4V, Johnson Holmquist for SiC, Johnson Cook for Al5083-H116. .

3. Results and Discussion

In Figure 3a, the velocity change of the projectile can be seen for 5mm SiC/0, 10, 15, 20, 25, and 30 mm Al5083-H116 laminated composite armors. With a small loss of velocity, the bullet pierced the 5 mm thick SiC tile at ~ 10 μs. Laminated composites with 10, 15, 20, and 25 mm thick Al5083-H116 backing armors were perforated by ".30 APM2" at approximately 45, 50, 65, and 80 μs, respectively. The velocity drop of the projectiles in the range of 0-15 μs, were calculated similarly for all laminated composite armors. Penetration stages of the projectile in the 5 mm SiC/30 mm Al5083 laminated composite armor plate is given in Figure 4b. In this figure, deformations occurring in the range of 0-12.005 μs can be seen in the projectile and laminated composite armor. As can be seen from this figure, 0-15 μs was the time interval during which the deformation of the projectile nose and the formation of ceramic fracture conoid was formed. The phenomenon of the ceramic cone is the main reason for the ballistic success of ceramic/metal composite armor plates [23-25].

Fracture conoid spreads ballistic energy over a larger area on the backing plate. As a result, elastic and plastic work increases. Also, with the use of high hardness ceramic front layer, the projectile loses its ballistic efficiency and penetration ability as a result of deformation on the projectile nose. In some cases, the projectile breaks into pieces and kinetic energy decreases as a result of mass loss. As a result, ceramic/metallic laminations both reduce the kinetic energy of the projectile and increase the energy required for perforation. In all analyzes carried out, the formation of the ceramic cone was fully modeled. Thanks to the ceramic cone formation, 5 mm SiC/30 mm Al5083-H116 laminated composite armor stopped ".30 APM2" projectile at ~94 μs.

The backing plate is brittle but high strength or ductile but low strength has negative consequences for ballistic protection. The brittle backing plate breaks into several pieces after a ballistic collision. The low-strength, tough backing plate does not show sufficient ballistic strength and is perforated by the projectile Therefore, toughness and strength must be optimized for full ballistic strength [26]. For this reason, 5 mm SiC/Mg AZ31B armor against ".30 APM2" could provide full ballistic protection almost twice as thick as 5mm SiC/Al5083-H116 laminated composite armor. Figure 4a shows the velocity change of the bullet for 5mm SiC/0-55 mm Mg

Celal Bayar University Journal of Science
Volume 16, Issue 4, 2020, p 409-418
Doi: 10.18466/cbayarfbe.771866

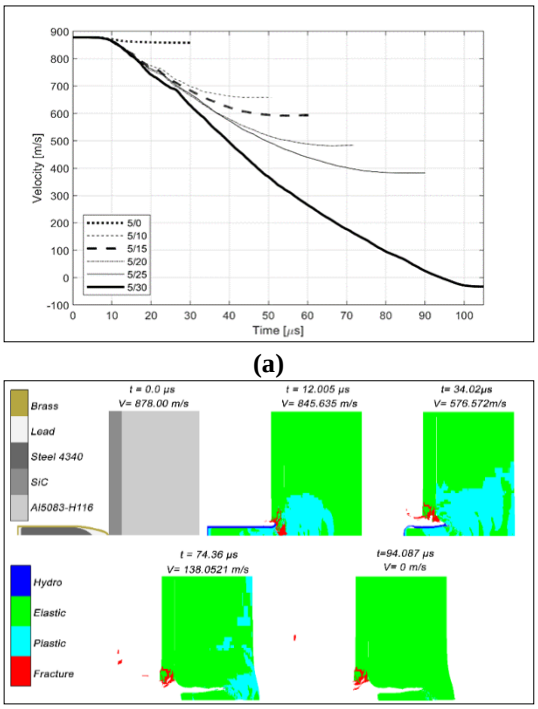

Figure 3. The velocity change of projectile as a function of time for 5 mm SiC/0-30 mm Al5083-H116 laminated composites (a) and penetration process of the projectile in 5 mm SiC/30 mm Al5083 laminated composite armor (b)

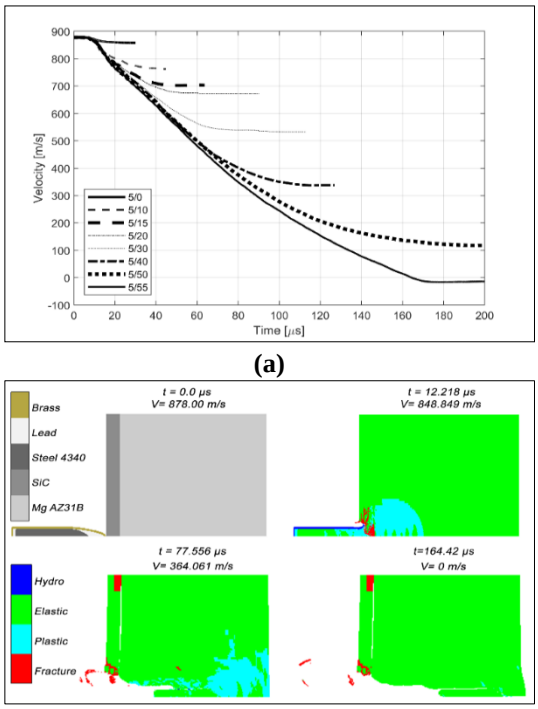

Figure 4. The velocity change of projectile as a function of time for 5 mm SiC/0-55 mm Mg AZ31B laminated composites (a) and penetration process of the projectile in 5 mm SiC/55 mm Mg AZ31B laminated composite armor (b)

AZ31B armor plates. The projectile was stopped at 164.42 μs using a 55 mm Mg AZ31B backing layer. Figure 6b shows the penetration of the projectile in 5 mm SiC/55 mm Mg AZ31B composite armor. In the first 12 μs, similar to the 5 mm SiC/30 mm Al5083-H116 composite armor, the velocity drop of the projectile was very low due to the low energy required for the fracture of the ceramic tile. In Fig. 4b, it is seen that the brass jacket of the projectile was stripped from the steel core.

Figure 5a shows the velocity change of the projectile for 5 mm SiC/0-10 mm Ti6Al4V armor. As shown in the graphic, the projectile was stopped at 61.3 μs by a 5 mm SiC/10mm Ti6Al4V composite armor. This thickness is less than half the limit thickness of the SiC/Al5083-H116 composite armor to protect against ".30 APM2" threat. Using Ti6Al4V, a 75 % thickness reduction was achieved compared to the Mg AZ31B backing layer. The penetration of the projectile in the 5 mm SiC/10 mm Ti6Al4V laminated composite armor plate is given in Fig.5b.

As a result of the bullet hitting the ceramic tile, a ceramic facture conoid was formed. As seen from the light blue colors representing plastic deformation, plastic deformations occurred in the bullet during penetration and the bullet was eroded.

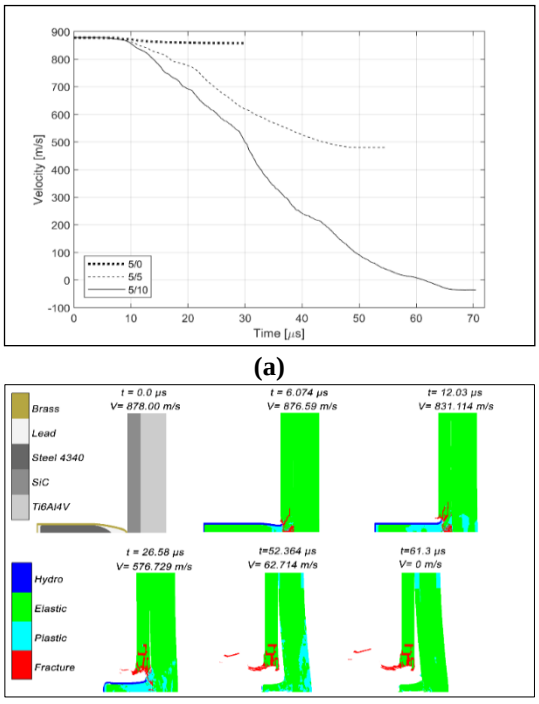

Figure 5. The velocity change of projectile as a function of time for 5 mm SiC/0-10 mm Ti6Al4V laminated composites (a) and penetration process of the projectile in 5 mm SiC/10 mm Ti6Al4V laminated composite armor (b)

Celal Bayar University Journal of Science
Volume 16, Issue 4, 2020, p 409-418
Doi: 10.18466/cbayarfbe.771866

Al5083-H116 and Mg AZ31B metallic armor plates were locally formed with plastic deformations, resulting in penetration and perforation in that local area. On the Ti6Al4V armor plate, plastic deformation and deflection occurred in almost the entire cross-sectional length. Thus, plastic work increased, and the kinetic energy of the bullet could be absorbed.

In Figure 6, residual velocities of the projectile are given for laminated composite armor with various thick Mg AZ31B, Al5083-H116 and Ti6Al4V backing layer. The projectile exited the unlayered 5mm SiC ceramic target at a speed of 858.11 m/s. Residual velocities of the projectile were calculated as 480.39 m/s of 5 mm SiC/5 mm Ti6Al4V composite armor target. From 5 mm SiC/10, 15, 20 and 25 mm Al5083-H116 composite targets, residual velocities of projectiles were respectively, 657.54, 591.7, 481. 87 and 382.57 m/s. After perforation of the 20 mm thick Al5083-H116 monolithic armor plate, the residual velocity of the projectile which had an initial velocity of 822.4 m/s was experimentally determined as 694.3 m/s by Borvik et al. [5]. In the same study, for 3x20 mm thick Al5083-H16 armor plates, the ballistic limit velocity of the APM2was reported as 901 m/s (calc) and 912 m/s (exp). In the analyzes, it was observed that 5 mm SiC/30 mm Al5083-H116 armors stopped ".30 APM2" with the first speed of 878 m/s. For 5 mm SiC/10, 15, 20, 30, 40 and 50 mm Mg AZ31B laminated composite targets, the residual velocity of the projectile was calculated as 762.41, 702.17, 672.79, 532.49, 337.91 and 119.19 m/s, respectively. In the previous study, it was determined that the limit speed of the ".30 APM2" bullet for the 86.48 mm thick Mg AZ31B armor plate was 863 m/s [7]. In this study, ".30 APM2" was stopped by a 5 mm SiC/55 mm Mg AZ31B target.

In Figure 7, some perforated laminated composite armor plates are given. The perforation type in 20 mm thick Al5083-H116 and Mg AZ31B backing layers, was ductile hole growth type. This type of puncture is especially seen in materials of medium hardness and thickness [27]. It was also found that the inlet hole was larger than the outlet hole, especially in the 20mm Al5083-H116 backing layer. This phenomenon occurs as a result of striping the brass jacket in a similar way in the literature [28, 29]. Ductile plugging type perforation occurred in a 5 mm SiC/5 mm Ti6Al4V armor plate. In Figure 8, plugging perforation stages and tensile stresses are given. In plugging type puncture, adiabatic shear bands occurring under the high strain rate of the material are effective. Another factor that causes this puncture type is a blunt bullet shape [27]. As a result, the bullet nose became blunt. After dishing, shearing and tensile stress occurred in the local area where the corners of the bullet nose touched the target (Fig. 8). The local area where tensile stress occurred was horizontally and circumferentially cracked. Finally, the target was perforated as a ductile plugging type.

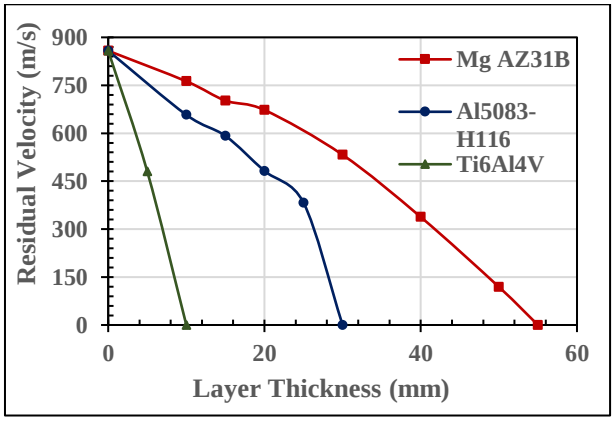

Figure 6. Residual velocity versus backing layer thickness for 5 mm SiC tiles backed with various light metal layers

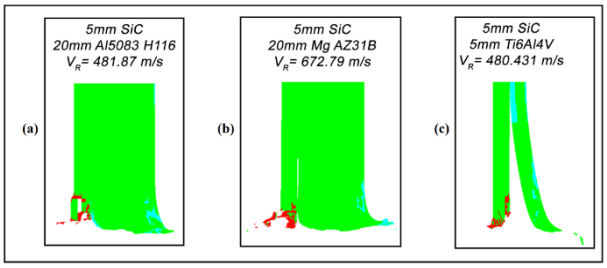

Figure 7. Perforation types of 5 mm SiC/light metal laminated composites: (a) 20 mm Al5083 H116, (b) 20 mm Mg AZ31B and (c) 5 mm Ti6Al4V backing layers

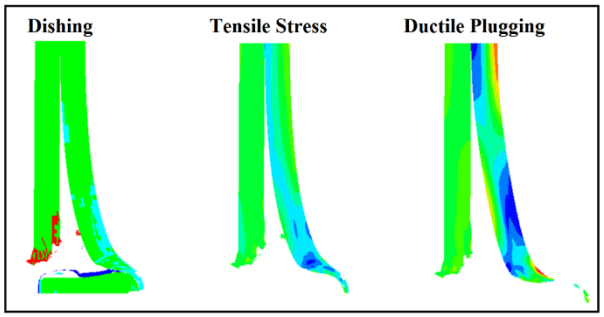

Figure 8. Perforation types of 5 mm SiC/light metal laminated composites: (a) 20 mm Al5083 H116, (b) 20 mm Mg AZ31B and (c) 5 mm Ti6Al4V backing layers

In Ti6Al4V alloy armors, petalling and especially plugging perforation types are determined as common puncture types[10].

In Figure 9a, the velocity change graphs of ".30 APM2" for 10 mm SiC /0-15 mm Al5083-H116 composite armors are given. After losing more than half of its velocity, 30 APM2 perforated composite armor at approximately 70 μs when 10 mm thick Al5083-H116 was used. When the backing layer thickness of Al5083-H116 was increased to 15 mm, the ".30 APM2" projectile was stopped by the composite armor plate at

Celal Bayar University Journal of Science
Volume 16, Issue 4, 2020, p 409-418
Doi: 10.18466/cbayarfbe.771866

96.2 µs. In Figure 9b, the penetration stages of the ".30 APM2" projectile in this armor plate can be seen. Compared to 5 mm SiC/Al5083-H116 composite armors, the ceramic fracture conoid formed in 10 mm SiC/15 mm Al5083-H116 composite armor was larger. Besides, as a result of the transfer of momentum from the fracture conoid base to the backing layer and the spread of the collision energy over a wider area, plastic deformation occurred on almost all of the front surface of the Al5083-H116 backing layer.

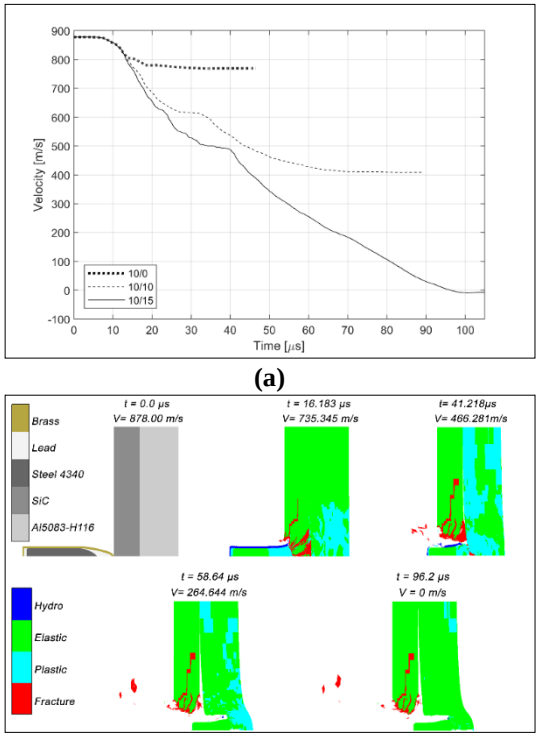

Figure 9. The velocity change of projectile as a function of time for 10 mm SiC/0-20 mm Al5083-H116 laminated composites (a) and penetration process of the projectile in 10 mm SiC/20 mm Al5083 laminated composite armor (b)

In Fig. 10a, the velocity change of the ".30 APM2" can be seen for 10 mm SiC/0-25 mm Mg AZ31B laminated composite armors. Composite armor using 10 mm Mg AZ31B as the backplate could not stop the projectile and the projectile perforated the armor at approximately 50 µs. When the Mg AZ31B backing layer thickness was 20 mm, the projectile was stopped at 176.15 µs. However, as seen in Fig. 10b, composite armor was perforated even though the bullet had stopped. Therefore, the analysis was carried out for 25 mm thick Mg AZ31B. In this analysis, it was calculated that the projectile was safely stopped by composite armor at 90.55 µs. To stop the ".30 APM2" projectile, it was determined that 5 mm SiC tile should be supported with 55 mm thick Mg AZ31B (Fig. 10). it can be seen in Fig 10c that compared to 5 mm SiC/55 mm MgAZ31B composite armor (Fig. 6b), the projectile is more eroded and deformed by 10 mm SiC/25 mm Mg AZ31B composite armor. As a result, the bullet lost its kinetic energy and perforation ability and could not pierce 25 mm thick Mg AZ31B armor.

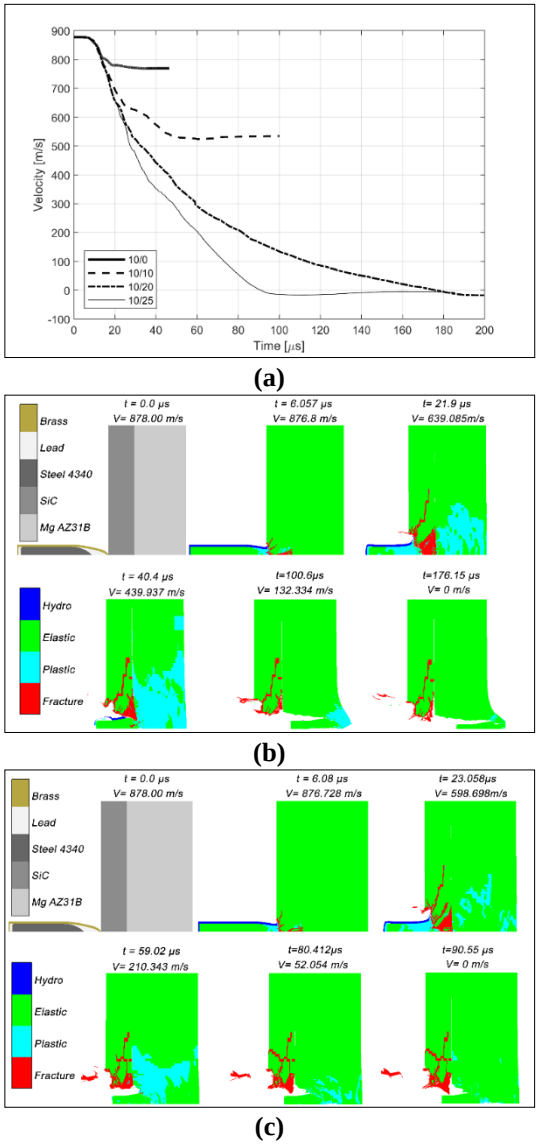

Figure 10. The velocity change of projectile as a function of time for 10 mm SiC/0-25 mm Mg AZ31B laminated composites (a), penetration process of the projectile in 10 mm SiC/20 mm Mg AZ31B (b) and 10 mm SiC/25 mm Mg AZ31B laminated composite armor (c)

In Figure 11a, the time-dependent velocity change of the ".30 APM2" projectile for the 10 mm SiC/10 mm Ti6Al4V composite armor is given. As can be seen in the graphic, the projectile was stopped by composite armor at about 88.18 µs. The projectile was eroded and deformed by the ceramic fracture conoid, which was well supported by the Ti6Al4V backing layer (Fig. 11b). Also, the mushrooming formation can be seen. Mushrooming is due to the difference between

Celal Bayar University Journal of Science
Volume 16, Issue 4, 2020, p 409-418
Doi: 10.18466/cbayarfbe.771866

projectile speed and penetration rate. Also, the mushrooming formation in the bullet can be seen. Mushrooming occurs when the projectile velocity is faster than the penetration velocity [15, 17, 19].

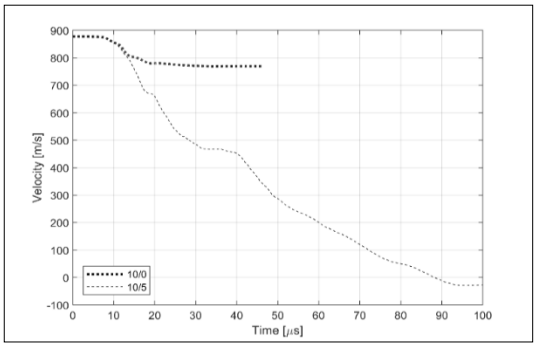

(a)

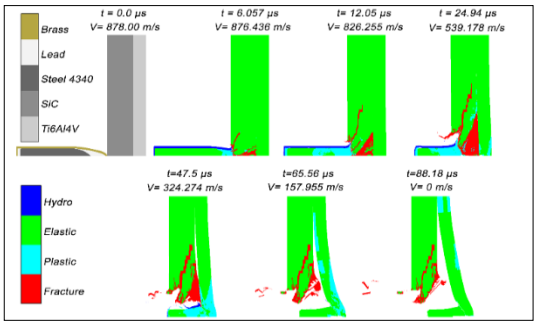

(b)

Figure 11. The velocity change of projectile as a function of time for SiC/Ti6Al4V laminated composites (a) and penetration process of the projectile in 10 mm SiC/5 mm Ti6Al4V laminated composite armor (b)

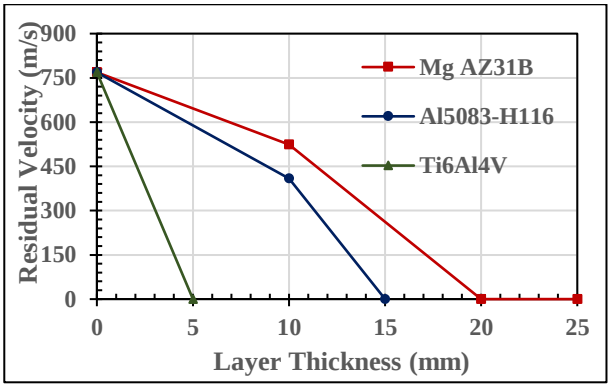

Figure 12. Residual velocity versus backing layer thickness for 10 mm SiC tiles backed with various light metal layers

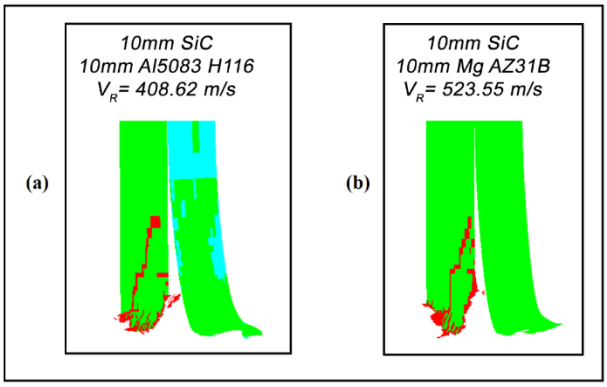

Figure 13. Perforation types of 10 mm SiC/light metal laminated composites: (a) 10 mm Al5083 H116 and (b) 10 mm Mg AZ31B

Table 3. Minimum areal densities for ballistic protection

Laminating Material and Configurations	Areal Density (kg/m^2)	Ammunition / Striking Velocity (m/s)	References
6 mm Alumina/12 mm Dual Phase Steel	100	7.62 x51 AP / -	[30]
20 mm Weldox	150	7.62 APM2 / 800	[28]
40 mm Al7075-T651	108	7.62 APM2 / 950	
Al7075-T0	85	7.62 x51 AP / -	[29]
AISI 4140	100		
3x20 mm Al5083-H116	162	7.62 APM2 / 914.5	[5]
50.93 mm Al5083-H113		.30 APM2 / 853	
76.48 mm Mg AZ31B	135.2	.30 APM2 / 863	[7]
17.22 mm Steel (RHA)		.30 APM2 / 914	
10 mm SiC/5 mm Ti6Al4V	54.245	.30 APM2 / 878	Present Study
5 mm SiC/10 mm Ti6Al4V	60.265		
10 mm SiC/15 mm Al5083-H116	72.65		
10 mm Si/25 mm MgAZ31B	76.65		
5 mm SiC/30 mm Al5083-H116	97.075		
5 mm SiC 55 mm MgAZ31B	113.975		

The residual velocities of ".30 APM2" projectiles for different backing layer material and thickness are given in Figure 12. The projectile perforated the composite armor using the 10 mm Al5083-H116 backing layer at 408.62 m/s. During penetration, as a result of the projectile blunting, a dishing form was formed in the rear surface of the 10 mm Al5083-H116 layer. In the later stages of penetration, a hole was formed in the middle of this dishing and composite armor was perforated (Fig. 13a). In composite armor where a 10 mm Mg AZ31B backing layer was used, the residual velocity of the projectile was calculated as 523.55 m/s. Ductile hole growth type puncture occurred in the armor plate of Mg AZ31B (Fig 13b).

In Table 3, the areal densities of the armors providing ballistic protection are given. In this study, the lowest areal density values were obtained in laminated composites using the Ti6Al4V backing layer. Using layered SiC/Ti6Al4V armor, weight was reduced by 55-60% compared to monolithic RHA armor. By layering Mg AZ31B with a 10 mm SiC tile, a weight reduction of about 40% was achieved compared to monolithic Mg AZ31B and RHA. Al5083-H116 armor layered with 10mm SiC tile provided ballistic protection 55 % lighter than monolithic Al5083-H116 and 45% lighter than monolithic RHA

4. Conclusion

In this study, the ballistic performance of composite armors obtained by layering Al5083-H116, Mg AZ31B and Ti6Al4V light metals with 5 and 10 mm SiC tiles were investigated as analytically. The results obtained are as follows:

1. The most important role of the ceramic layer in increasing the ballistic strength of composite armor is fracture conoid failure. This damage and its effect were excellently modeled determined with SPH.
2. The ceramic fracture conoid should be supported by a backing layer that has a good combination of high strength and toughness to fully demonstrate the effect of ballistic strength. Therefore, the best ballistic performance exhibited SiC/Ti6Al4V composite armor.
3. By using Al 5083-H116, Mg AZ31B and Ti6Al4V light metal alloy and SiC front layer, the similar ballistic protection was achieved with 45-60% lighter composite armors compared to the monolithic RHA armor
4. The lowest areal density which ballistic protection was provided was calculated as 54.245 kg/m^2 in 5 mm SiC/10 mm Ti6Al4V composite armor.
5. SiC/Al5083-H116 and SiC/Mg AZ31B layered composite armors provided the same ballistic protection approximately 50 % thinner than monolithic armors of the same metals.
6. SiC/Al5083-H116 and SiC/Mg AZ31B layered composite armor plates provided the same ballistic protection approximately 50 % thinner than monolithic armors of the same metals.
7. Perforation types were determined as ductile hole growth in Al5083-H116 and Mg AZ31B, and as ductile plugging in Ti6Al4V.

Author's Contributions

Saim Kural: edited the revisions, performed the analysis and result analysis
Mehmet Ayvaz: Drafted and wrote the manuscript Assisted in result interpretation and helped in manuscript preparation.

Ethics

There are no ethical issues after the publication of this manuscript.

References

1. P.K. Jena, B. Mishra, K.S. Kumar, T.B. Bhat, An experimental study on the ballistic impact behavior of some metallic armour materials against 7.62 mm deformable projectile, *Materials & Design*. 31 (2010) 3308-3316. https://doi.org/10.1016/j.matdes.2010.02.005

2. M.K. Forrestal, V.K. Luk, Perforation of aluminum armor plates with conical-nose projectiles. *Mechanics of Materials*. 10(1-2) (1990) 97-105. https://doi.org/10.1016/0167-6636(90)90020-G

3. T. Borvik, A.H., Clausen, O.S., Hopperstad, Langseth, M., Perforation of AA5083-H116 aluminium plates with conical-nose steel projectiles—experimental study, *International Journal of Impact Engineering*. 30 (2004) 367-384. https://doi.org/10.1016/S0734-743X(03)00072-1

4. T. Borvik, M.J. Forrestal, O.S. Hopperstad, T.L. Warren, Langseth, M., Perforation of 5083-H116 aluminum plates with conical-nose steel projectiles-calculations, *International Journal of Impact Engineering*. 36 (2009) 426-437. https://doi.org/10.1016/j.ijimpeng.2008.02.004

5. T. Borvik, M.J. Forrestal, T.L. Warren, Perforation of 5083-H116 aluminum armor plates with ogive-nose rods and 7.62 mm APM2 bullets, *Experimental Mechanics*. 50 (2010) 969-978. https://doi.org/10.1007/s11340-009-9262-5

6. M.F. Abdullah, S. Abdullah, M.Z. Omar, Z. Sajuri, M. Sohaimi, Failure observation of the AZ31B magnesium alloy and the effect of lead addition content under ballistic impact, *Advances in Mechanical Engineering*. 7(5) (2015) 1-13. https://doi.org/10.1177/1687814015585428

7. T.L. Jones, R.D. DeLorme, M.S. Burkins, W.A. Gooch, Ballistic performance of magnesium alloy AZ31B. *23rd International symposium on ballistics*. 989-995, 16-20 April 2007, Tarragona, Spain.

8. J.S. Montgomery, M.G.H. Wells, B. Roopchand, J.W. Ogilvy, Low-cost titanium armors for combat vehicles, *JOM*. 49(5) (1997) 45-47. https://doi.org/10.1007/BF02914684

9. G. Sukumar, B.B. Singh, A. Bhattacharjee, K. Sivakumar, A.K. Gogia, Effect of heat treatment on mechanical properties and ballistic performance of Ti-4Al-2.3V-1.9Fe alloy, *Materials*

Today. 2 (2015) 1102-1108. https://doi.org/10.1016/j.matpr.2015.07.015

10. B.B. Singh, G. Sukumar, A. Bhattacharjee, K.S. Kumar, T.B. Bhar, A.K. Gogia, Effect of heat treatment on ballistic impact behavior of Ti–6Al–4V against 7.62 mm deformable projectile, *Materials & Design*. 36 (2012) 640-649. https://doi.org/10.1016/j.matdes.2011.11.030

11. L.S. Gallo, M.O.C.V. Boas, A.C.M. Rodrigues, F.C.L. Melo, E.D. Zanotto, Transparent glass–ceramics for ballistic protection: materials and challenges, *Journal of Materials Research and Technology*. 8(3) (2019) 3357–3372. https://doi.org/10.1016/j.jmrt.2019.05.006

12. A.L. Florence, Interaction of projectiles and composite armour, part II. Standard Research Institute, Menlo Park, California, 1969.

13. V.P. Alekseevskii, Penetration of a rod into a target at high velocity. *Combustion, Explosion and Shock Waves*. 2(2) (1966) 63-66. https://doi.org/10.1007/BF00749237

14. Tate, A., A theory for the deceleration of long rods after impact, *Journal of the Mechanics and Physics of Solids*. 15(6) (1967) 387–399. https://doi.org/10.1016/0022-5096(67)90010-5

15. R.L. Woodward, A simple one-dimensional approach to modelling ceramic composite armour defeat, *International Journal of Impact Engineering*. 9(4) (1990) 455-474. https://doi.org/10.1016/0734-743X(90)90035-T

16. P.C. Den Reijer, Impact on ceramic faced armours. PhD thesis, Delft University of Technology, 1991.

17. R. Zaera, V. Sanchez-Galvez, Analytical modeling of normal and oblique ballistic impact on ceramic/metal lightweight armours, *International Journal of Impact Engineering*. 21(3) (1998) 133–148. https://doi.org/10.1016/S0734-743X(97)00035-3

18. I.S. Chocron Benloulo, V. Sanchez-Galvez, A new analytical model to simulate impact onto ceramic/composite armors, *International Journal of Impact Engineering*. 21(6) (1998) 461–471. https://doi.org/10.1016/S0734-743X(98)00006-2

19. S. Feli, M.E.A Aaleagha, Z. Ahmadi, A new analytical model of normal penetration of projectiles into the light-weight ceramic–metal targets, *International Journal of Impact Engineering*. 37(5) (2010) 561–567. https://doi.org/10.1016/j.ijimpeng.2009.10.006

20. E. Medvedovski, Ballistic performance of armour ceramics: Influence of design and structure. Part 2, *Ceramics International*. 36 (2010) 2117-2127. https://doi.org/10.1016/j.ceramint.2010.05.022

21. M.R.I. Islam, J.Q. Zheng, R.C. Batra, Ballistic performance of ceramic and ceramic-metal composite plates with JH1, JH2 and JHB material models, *International Journal of Impact Engineering*. 137 (2020) e103469. https://doi.org/10.1016/j.ijimpeng.2019.103469

22. G. R. Johnson, W. H. Cook, A constitutive model and data for metals subjected to large strains, high strain rates and high temperatures, Proceedings of the *7th International Symposium on Ballistics*,1983.

23. M. Übeyli, R.O. Yildirim, B. Ögel, Investigation on the ballistic behavior of Al2O3/Al2024 laminated composites, *Journal of Materials Processing Technology*. 196 (2008) 356-364. https://doi.org/10.1016/j.jmatprotec.2007.05.050

24. C.C. Holland, E.A. Gamble, F.W. Zok, V.S. Deshpande, R.M. McMeeking, Effect of design on the performance of steel-alumina bilayers and trilayers, *Mechanics of Materials*. 91(1) (2015) 241-251. https://doi.org/10.1016/j.mechmat.2015.05.002

25. B. Wang, G. Lu, On the optimisation of two-component plates against ballistic impact, J. *Journal of Materials Processing Technology*. 57 (1996) 141-145. https://doi.org/10.1016/0924-0136(95)02050-0

26. T. Demir, M. Übeyli, R.O. Yildirim, M.S. Karakas, Response of Alumina/4340 Steel Laminated Composites against the Impact of 7.62 mm Armor Piercing Projectiles, *Science and Engineering of Composite Materials*. 16(2) (2009) 89-98. https://doi.org/10.1515/SECM.2009.16.2.89

27. M.E. Backman, W. Goldsmith, The mechanics of penetration of projectiles into targets. *International Journal of Engineering Science*. 16(1) (1978) 1-99. https://doi.org/10.1016/0020-7225(78)90002-2

28. E.A., Flores-Johnson, M., Saleh, L., Edwards, Ballistic performance of multi-layered metallic plates impacted by a 7.62-mm APM2 projectile, *International Journal of Impact Engineering*. 38 (2011) 1022-1032. https://doi.org/10.1016/j.ijimpeng.2011.08.005

29. T. Demir, M. Übeyli, R.O. Yıldırım, Investigation on the ballistic impact behavior of various alloys against 7.62 mm armor piercing projectile, *Materials & Design*. 29 (2008) 2009-2016. http://doi.org/10.1016/j.matdes.2008.04.010

30. M. Übeyli, H. Deniz, T. Demir, B. Ögel, B. Gürel, Ö. Keleş, Ballistic impact performance of an armor material consisting of alumina and dual phase steel layers, *Materials & Design*. 32(3) (2011) 165-1570. https://doi.org/10.1016/j.matdes.2010.09.025